Density Functional Study of Magnetic Coupling Parameters: F and H Hyperfine Splitting Constants for the Prototype Inorganic (d^1) and Organic (p^1) Radicals TiF_3 and CH_3

Paola Belanzoni,[†] Evert Jan Baerends,*[,‡] and Michiel Gribnau[§]

Dipartimento di Chimica, Universita di Perugia, Via Elce di Sotto 8, 06123 Perugia, Italy, Theoretical Chemistry Department, Free University, De Boelelaan 1083, 1081 HV Amsterdam, The Netherlands, and Unilever Research Laboratorium, Olivier van Noortlaan, Vlaardingen, The Netherlands

Received: September 28, 1998; In Final Form: February 17, 1999

Hyperfine splittings (hfs) are calculated for the title compounds. These calculations resolve the discrepancy found earlier[1] between the calculated and experimental hfs for F in TiF_3 by (a) careful consideration of the spin polarization effects in the occupied 2s and 2p shells, as well as the nonnegligible spin polarization of the 1s shell, and (b) reconsideration of the experimental results by redefining the relative signs of the principal values of the *A* tensor on the basis of the calculations. The presently available density functionals (LDA, GGA's) are shown to yield fair agreement for the magnetic coupling parameters, indicating the usefulness of the DFT calculations for interpretation of ESR data of large complexes. Such interpretation is difficult on the basis of the experimental hfs data only, due to the intricacies of the spin polarization mechanism that gives rise to them.

1. Introduction

Hyperfine splittings in ESR spectra of transition metal complexes with an unpaired electron are often used to obtain detailed information on the electronic structure. The sensitivity of the technique also makes it very suitable for the study of metallic centers in large molecules of biological interest, in particular active centers in enzymes. In view of their computational efficiency, DFT methods are suitable for such large systems. It is therefore useful to establish the level of accuracy that can be attained with present day functionals for the magnetic parameters. We have previously studied magnetic coupling parameters for the TiF_3 complex[1] with D_{3h} symmetry. In that work we were mainly dealing with the *g* tensor and with the Ti hyperfine splitting. Although it had been deduced from the experiments that the unpaired electron in the TiF_3 complex had mostly 4s character, the calculations proved it to be mostly 3d. This apparent contradiction between experiment and theory was resolved by explicit calculation of the *g* and *A* tensors for titanium, which showed that an unpaired electron of 3d character, as resulted from our calculations, could also lead to the observed magnetic data. The approximations that usually have to be made in the deductions from experiment were critically analyzed, and the conclusion has been that they can be erroneous and need to be verified by electronic structure calculations. It is, indeed, a combination of experiments with theoretical calculations that will afford a reliable interpretation of the experimental magnetic coupling data in terms of the electronic structure.

It is of course a prerequisite that the calculations are sufficiently accurate. In the context of the previous work we also reported the theoretically calculated *A* tensors (both the contributions from the dipolar operator and the Fermi contact term) for the fluorine nuclei, using both spin restricted and spin unrestricted calculations. These results are reproduced here in Table 1. The *A* tensor values due to the F nuclei are small if compared to the calculated atomic fluorine values ($A_{iso} = 6374$ MHz, $A_{dip} = 1/3(A_\perp - A_{||}) = 5138$ MHz for a $(2p_z)^1$

TABLE 1: Theoretical Magnetic *A* Tensors for TiF_3[d]

	A tensor		
	along bond (F),[a] A_{bond}	normal to bond (F),[a] $A_\perp$	along *z*-axis (F),[a] A_{zz}
	Restricted		
first order	33.5	−18.4	−14.9
second order	−2.5	8.2	2.7
total dipolar	31.0	−10.2	−12.2
pseudocontact		2.9	
A_{Fermi}		28.1	
total A_{iso}[b]		31.0	
total *A*	59.1	17.9	15.9
	Unrestricted		
first order	33.6	4.4	−38.1
second order	−1.7	5.7	1.8
total dipolar	31.9	10.1	−36.3
pseudocontact		1.9	
A_{Fermi}		−44.6	
total A_{iso}[b]		−42.7	
total *A*	−12.7	−34.5	−80.9
	Experimental[c]		
A_{iso}		|23.6|	
total *A*			
neon	|11.5|	|11.5|	|47.9|
argon	|10.3|	|10.3|	|44.7|

[a] The following calculated *A* values represent the first order, the second order and the sum of the two terms (total dipolar), without the Fermi contact contribution but including an isotropic "pseudocontact" contribution that arises in the second order and is also given separately. [b] The contributions to A_{iso} are the pseudocontact second-order term and the Fermi contact term (A_{Fermi}). [c] As reported in ref 2. The experimental A_{iso} value is derived on the assumption of positive signs of all principal *A* tensor values. [d] All *A*-tensor values are expressed in MHz. The basis set we used is the DZ (1s frozen) basis set as described in Table 2.

[†] Universita di Perugia.
[‡] Free University.
[§] Unilever Research Laboratorium.

10.1021/jp983891u CCC: $18.00
Published on Web 04/22/1999

configuration). This is a consequence of there being only little (3%) fluorine $2p_\sigma$ (along the Ti−F bond) character in the MO containing the unpaired electron. There were several unsatisfactory features regarding the calculations for the F hyperfine splitting, while also the experimental situation was not completely clear, hampering the analysis. In the first place we note in Table 1 the large difference between the restricted and unrestricted results, not only in the dipolar part but also in the Fermi contact term, which even changes sign, from +28.1 MHz in the restricted to −44.6 in the unrestricted case. There is only a small isotropic contribution from the second-order contributions of the dipolar part, listed as the pseudocontact term in the table, so the total isotropic *A* value is close to the Fermi contact term. The unrestricted calculation differs considerably from the experimental A_{iso}, given as 23.6 MHz (see below however for a reassesment of the experimental result). Second, we noted the departure from axial symmetry of the calculated *A* tensor, while the experimental fluorine *A* tensor had been determined assuming an axial (along *z*-axis) spin Hamiltonian.[2] Axial means that there is a distinct A_{zz} component, the *z*-axis being perpendicular to the molecular plane, while the A_{xx} and A_{yy} components are equal. This implies that the *A* tensor is assumed diagonal with equal *x* and *y* components at each F. The symmetry of the system only dictates the *A* tensor to be diagonal when the *x* and *y* axes are chosen along the Ti−F bond and perpendicular to it, while the components may all differ. As a matter of fact, the calculated *A* tensor on F had, indeed, three different components. Again, the pattern is rather different for the restricted and unrestricted calculations (see Table 1), the former having the largest component (59.1 MHz) along the Ti−F bond, the latter having the largest component along the *z*-axis (−80.9). The restricted and unrestricted results differ not only from each other but they also both differ from experiment. For instance, the presumably most reliable unrestricted value for the *z* component of −80.9 MHz does not compare particularly well with the corresponding experimentally established value of |47.9| or |44.7| MHz. It should of course be kept in mind that the spin densities, and therefore the hyperfine splittings, are very small, so even small absolute errors lead to large percentage errors.

It is important to try to sort out the problems with the ligand hyperfine splitting in TiF_3. Ligand hyperfine splittings (often small) are important spectroscopic data to monitor the electronic structure of TM complexes, including systems of biological interest, cf. refs 3 and 4 and references therein. Density functional calculations have proven to give very accurate results for isotropic hyperfine coupling constants of small organic radicals, cf. refs 5−10, of comparable accuracy to ab initio calculations including sophisticated electron correlation treatments, cf. refs 12 and 14−17 and refs 18 and 19 and references therein. Reports on hyperfine splitting calculations on TM complexes using DFT give a mixed picture, with results being sometimes reasonable and sometimes less satisfactory. It has been suggested that less satisfactory results of DFT calculations, at least those that employ density functionals that are in common use, are due to wrong metal−ligand covalencies. Such observations have been made for the DFT hyperfine structure for a series of molybdenum(V) oxyhalide anions,[20] which have relevance to the active site of molybdenum oxidoreductase enzymes, and for a series of model sites of plastocyanin,[21] a blue-copper protein. The results did not provide accurate estimates of the experimentally determined *g* and *A* values. On the other hand, exchange-only DFT (Xα-LCAO) calculations on the electronic structure and magnetic coupling parameters of the Cu(II) bis(dithiocarbamate) complex[22] gave fair agreement with the experimental EPR results, indicating the bonding between the Cu atom and the four ligand S atoms was mainly covalent. Satisfactory results were also obtained for a multinuclear organometallic complex with DFT-GGA calculations.[23]

The TiF_3 complex will be used here as a further test case for the accuracy of the density functional approach for calculating magnetic coupling parameters. At the theoretical side we will establish to what extent spin polarization effects play a role. Since there are essentially fully occupied 2p and 2s shells on the F ligands, spin polarization effects will be significant. Polarization of the 2p shell strongly affects the dipolar (traceless) part of the tensor, whereas spin polarization of the 2s shell affects the Fermi contact term. Even though the 1s shell is rather tight in F, it will be shown that spin polarization of this shell contributes to the Fermi contact term. We will also have to address the experimental situation. The discrepancy between experiment and theory will prove to be only apparent. The experimental spectrum of fluorine in TiF_3 could not completely solve the F *A* tensor, and an axial spin Hamiltonian was then assumed to determine the values of the *A* tensor. The signs of these principal values could not be assigned, and the isotropic part of the fluorine *A* tensor was derived by assuming the same sign for all the principal values of the hyperfine tensor. However, the participation of the fluorine $2p_\sigma$ orbitals (directed along the Ti−F bond) in the MO containing the unpaired electron suggests an axial *A* tensor with main axis along a Ti−F bond (the *x*-axis for fluorine atom number 1, F^1) and possibly equal A_{zz} and A_{yy} components (this would hold for a purely $2p_\sigma$ unpaired electron). The assumption of an axial *A* tensor for fluorine oriented along the *z*-axis is therefore questionable. Actually, in the experimental spectrum more than the four lines that would be expected if $A_{xx} = A_{yy}$ ($= A_\perp$), are observed in the "perpendicular" part of the spectrum around $g_\perp$. We will reconsider this issue and will investigate the agreement between calculated and experimental spectra by running computer simulations of the experimental spectrum with calculated values for the tensor components.

We have included in our investigation the trigonal planar CH_3 radical, since this system has some correspondence to TiF_3, also having the spin density mainly on the central atom and having a H spin density that has to derive from spin polarization effects. There are of course interesting differences too (H is in a nodal plane of the zero order spin density, H has no polarizable core, the unpaired spin has carbon $2p_z$ character rather than Ti $3d_{z^2}$, etc.). CH_3 is however particularly interesting since it is a well studied prototype system for which the mechanism of H hyperfine splitting in aromatic radicals is commonly illustrated. We can compare to previous calculations of the isotropic hyperfine splitting constants, and the full *A* tensor. Even for CH_3, caution is needed when comparison is made between calculated and experimental hyperfine coupling parameters. Significant vibrational corrections to the carbon isotropic coupling constant have been estimated[18] which imply that significant corrections have to be made to the direct experimental results[24] in order to make them comparable to a calculation on a static D_{3h} radical.

2. Computational and Methodological Details

Calculations were performed on the TiF_3 and CH_3 systems using the Amsterdam density functional (ADF)[25−27] and the companion GATENQ program packages[22,28−30] previously described.[1] The molecular orbitals were expanded in a basis set of Slater-type orbitals (STOs).[31] The frozen core approxima-

TABLE 2. Orbital Expansion Bases (all STO's) Used in Different Calculations for TiF_3

	fluorine									titanium	
						Basis					
	DZ	TZ	ae^A	ae^B	ae^C	ae^D	ae^E	ae^F	ae^G	TZ	ae^B
1s	frozen	frozen	8.33	7.70	7.33	7.16	7.33	7.33	7.33	frozen	9.00
1s				10.88	8.75	8.66	8.75	11.15	8.75		20.10
1s					11.15	12.99	11.15	14.92	11.15		26.30
1s					14.92		14.02		14.02		40.00
2s	1.92	0.74	0.74	0.74	1.75	1.72	1.70	1.75	1.70	frozen	5.60
2s	3.22	1.94	1.94	1.94	2.49	2.40	2.31	2.49	2.31		8.30
2s		3.24	3.24	3.24	3.85	3.72	3.43	3.85	3.43		
2s							4.95		4.95		
3s										3.10	2.95
3s										4.75	4.65
4s										0.80	0.80
4s										1.20	1.20
4s										1.90	1.90
2p	1.48	1.24	1.24	1.24	1.26	1.26	1.26	1.26	1.26	frozen	7.35
2p	3.52	2.30	2.30	2.30	2.36	2.36	2.36	2.36	2.36		12.00
2p		4.54	4.54	4.54	4.62	4.62	4.62	4.62	4.62		
2p									8.50		
2p									18.00		
3p										2.50	2.45
3p										4.05	4.05
3d										1.04	1.04
3d										2.30	2.30
3d										4.95	4.95
						Polarization Functions					
3d	2.00	2.00	2.00	2.00	2.00	2.00	2.00	2.00	0.50		
3d									2.00		
3d									4.50		
3d									27.00		
4p										1.20	1.20

tion is applied initially and subsequently relaxed. The parametrization of electron gas data by Vosko, Wilk, and Nusair[32] was used for the local density approximation (LDA) calculations. We also included nonlocal corrections to the exchange and correlation potentials. The generalized gradient corrections (GGA's) of Becke[33] for exchange and of Perdew[34,35] for correlation, termed BP, the corrections of Perdew and coworkers[36] for both exchange and correlation, termed PW91, and the corrections of Perdew and Wang[37] for exchange and Perdew[34,35] for correlation, termed PW86, were employed. The spin unrestricted approach has been applied in order to investigate the polarization effects. A description of the basis sets we used in TiF_3 and CH_3 calculations can be found in Tables 2 and 3, respectively. Core orbitals were frozen for Ti 1s−2p (exponents of the core orthogonalization functions: 1s 17.35, 2s 7.50, 2p 8.95), F 1s (exp 8.33), C 1s (exp 5.40), O 1s (exp 7.36), and N 1s (exp 6.38). More extensive basis sets were employed, also in all-electron calculations, to investigate the effect of the basis and of the frozen core approximation on the values of the *A* tensor terms (contact and dipolar) for the molecules. The implementation of the analytical gradient of the energy in ADF[38] allowed for a geometry optimization of the molecules. All the optimal geometries were obtained including Becke[33] and Perdew[34,35] nonlocal corrections in the calculations. The organic radical CH_3 adopts D_{3h} symmetry and the C−H distance turned out to be 1.0896 Å.

The ESR *g* and *A* tensors of the considered systems, containing each one unpaired electron and two (or more) nuclei with a magnetic moment, have been calculated by means of conventional second-order perturbation theory.[22,28,39] The following expressions for the *g* and *A* tensors may be written in the spin restricted case, i.e., α and β spin orbitals identical, an unpaired electron in orbital ϕ_n, and ϕ_n^k the part of ϕ_n centered at nucleus *k*:

$$g_{ij} = g_e\delta_{ij} + g_e \sum_{m(\neq n)} \sum_k \sum_{k'} \frac{\langle \phi_n^k | \xi_k(r^k) L_i^k | \phi_m^k \rangle \langle \psi_m | L_j^{k'} | \phi_n^{k'} \rangle}{\epsilon_n - \epsilon_m} \quad (1)$$

$$A_{ij}^k = P\left\langle \phi_n^k \left| \frac{F_{ij}^k}{(r^k)^3} \right| \phi_n^k \right\rangle + 2P \sum_{k' \neq k} \left\langle \phi_n^{k'} \left| \frac{F_{ij}^k}{(r^k)^3} \right| \phi_n^k \right\rangle + P \sum_{k' \neq k} \left\langle \phi_n^{k'} \left| \frac{F_{ij}^k}{(r^k)^3} \right| \phi_n^{k'} \right\rangle + P\left\{ \sum_{m \neq n} \frac{2\{\sum_k \langle \phi_n^k | \xi_k(r^k) L_i^k | \phi_m^k \rangle\} \left\langle \phi_m^k \left| \frac{L_j^k}{(r^k)^3} \right| \phi_n^k \right\rangle}{\epsilon_n - \epsilon_m} + \sum_{m \neq n} \sum_{p,q} \frac{i\epsilon_{ipq}\{\sum_k \langle \phi_n^k | \xi_k(r^k) L_p^k | \phi_m^k \rangle\} \left\langle \phi_m^k \left| \frac{F_{qj}^k}{(r^k)^3} \right| \phi_n^k \right\rangle}{\epsilon_n - \epsilon_m} \right\} \quad (2)$$

For the meaning of the symbols entering these expressions we refer to the previous paper[1] where they are explained in detail. However, it is useful to recall that the first three terms in the A_{ij}^k expression constitute the first-order dipolar contribution. They are split into a one-center term, with the dipolar operator and the basis functions all centered at the same nucleus *k*, and two two-center terms. One two-center term refers to the operator and one of the basis functions having their origin at the same center, and the other two-center term arises when the dipolar operator is centered on *k*, the basis functions being both centered on another nucleus *k*′. These two-center terms are often negligible but may be expected to be important in the case at hand, where we are interested in the hyperfine splitting of the

TABLE 3. Orbital Expansion Bases (all STO's) Used in Different Calculations for CH_3

	C	H	C	H
		Basis		
	DZ	DZ	ae[A]	ae[A]
1s	frozen	0.76	5.41	0.69
1s		1.28	9.29	0.92
1s				1.58
2s	1.24		1.06	
2s	1.98		1.52	
2s			2.68	
2s			4.20	
2p	0.96		0.98	1.25
2p	2.20		1.44	
2p			2.60	
2p			6.51	
		Polarization Functions		
2p		1.25		
3d	2.20		2.12	2.50
3d			3.71	

F nucleus (k = F), while the spin density is mainly on the neigbouring Ti atom (k' = Ti). The remaining terms are the second-order terms, which may have small isotropic contributions. Summing the first and second-order contributions to the A_{ij}^k tensor for nucleus k we obtain the total A tensor arising from the dipolar operator. For a fluorine nucleus in TiF_3 we may write the A tensor in an axis system with the x-axis along the Ti−F bond, the y-axis perpendicular to it in the plane of the molecule, and the z-axis perpendicular to the molecular plane, as follows:

$$A = \begin{vmatrix} A_{\text{bond}} & 0 & 0 \\ 0 & A_{\perp} & 0 \\ 0 & 0 & A_{zz} \end{vmatrix}$$

where A_{bond} represents the component along the Ti−F bond, $A_{\perp}$ is the component normal to the Ti−F bond in the plane of the molecule, and A_{zz} indicates the component along the z-axis (alternatively denoted $A_{||}$). Apart from the dipolar contributions to the A tensor elements, there will also be a fully isotropic contribution (equal contribution to all three diagonal elements) coming from the Fermi contact term. The Fermi contact contribution, A_{contact} or A_{Fermi}, is in the restricted case equal to

$$A_{ii}^k = \frac{8\pi}{3} P|\psi_n(0)|^2$$

where n refers to the unpaired spin−orbital. In the unrestricted case the spin polarization of the occupied orbitals is taken into account by writing

$$A_{\text{contact}}(k) = \frac{8\pi}{3}\frac{\mu_0}{4\pi} g_e g_k \beta_e \beta_n \sum_m (n_m^{\alpha}|\psi_m^{\alpha}(0)|^2 - n_m^{\beta}|\psi_m^{\beta}(0)|^2)$$

or, explicitly,

$$A_{\text{contact}}(k) = \frac{8\pi}{3}\frac{\mu_0}{4\pi} g_e g_k \beta_e \beta_n \sum_m \sum_{\mu,\nu(onk)} (n_m^{\alpha} c_{\mu m}^{\alpha} c_{\nu m}^{\alpha} - n_m^{\beta} c_{\mu m}^{\beta} c_{\nu m}^{\beta})\chi_{\mu}^k(0)\chi_{\nu}^k(0) + 2\sum_m \sum_{k'(\neq k)} \sum_{\mu(onk)} \sum_{\nu(onk')} (n_m^{\alpha} c_{\mu m}^{\alpha} c_{\nu m}^{\alpha} - n_m^{\beta} c_{\mu m}^{\beta} c_{\nu m}^{\beta})\chi_{\mu}^k(0)\chi_{\nu}^{k'}(0)\Bigg]$$

where m refers to the occupied spin orbitals, n_m^{σ} indicates the occupation number and contributions with both basis functions on other nuclei (k' and k'') are not taken into account. Using STOs, only 1s functions are responsible for the electronic density on the nucleus; therefore, only terms of the form $\chi_{\mu}^k(0)\,\chi_{\nu}^k(0) = 1s^k \cdot 1s^k$ and $\chi_{\mu}^k(0)\chi_{\nu}^{k'}(0) = 1s^k \cdot \chi^{k'}{}_{\nu}(0)$ give contributions in the above expression.

The dipolar terms may be extended in the same way to take into account the spin polarization.

The isotropic (pseudocontact) contribution due to the second-order terms in A_{ij}^k must be added to the Fermi contact term in order to obtain the total A_{iso} term.

$$A_{\text{iso}} = A_{\text{Fermi}} + A_{\text{pseudocontact}} = \frac{1}{3}(A_{\text{bond}} + A_{\perp} + A_{zz})$$

For the calculation of the partial spin-orbit parameter ζ_{rs}, the value for the atomic spin orbit parameter ζ^a for the considered atom and for the atomic orbital $|a\rangle$ is required. We have used for the Ti and F spin−orbit coupling constants, the Ti^{3+} d^1 value λ = 208.2 cm^{-1}, and the F λ = 346.0 cm^{-1}, calculated employing fully relativistic numerical atomic calculations,[40] see ref 1. For the C spin−orbit coupling constant we have employed the empirical spin−orbit splitting λ = 28 cm^{-1}.[42] The nuclear g value for ^{47}Ti was taken as $g_k = -0.31532$, for ^{19}F as $g_k = +5.2576$, for ^{13}C as $g_k = +1.4048$, and for ^{1}H as $g_k = +5.58556$.[43]

We have run simulations of the experimental spectrum with the CWR 1.1.3 program[41] for ^{48}Ti (I = 0) and ^{19}F (I = 1/2) nuclei. The total system consists of one electron spin (S = 1/2) and three nuclear spins (I = 1/2). The spectra were computed by addition of the spectra of 6400 different orientations (random) on a sphere. Each spectrum was calculated using full matrix diagonalization of the spin Hamiltonian. Simulations have been performed with both the parameters proposed originally[2] and parameter sets from various types of calculations (spin restricted and unrestricted, frozen core and all electron).

3. Results

3.1. Fluorine Hyperfine Couplings. The ESR spectra of the TiF_3 molecule trapped in argon and in neon matrixes at 4−10 K have been recorded by T. C. DeVore and W. Weltner, Jr. and are shown in Figures 1−3 of ref 2. The most conspicuous features of the experimental spectrum are the following. First, a set of four strong lines is observed around 3350 G, with intensity distribution 1:3:3:1, which have been attributed to hyperfine splitting due to three equivalent F nuclei (I = 1/2). By symmetry, the A and g tensors have, in the molecular frame with z-axis perpendicular to the molecular plane, a block structure, with there being no coupling between the zz (also denoted ||) component and the x,y block (the ⊥ components). In this case, the spectrum of a sample with randomly oriented TiF_3 molecules yields a "parallel part", where the lines center around $g_{||}$ and show a splitting governed by $A_{||}$ (=A_{zz}) and the number of equivalent nuclei. The typical four-line pattern with intensity ratio 1:3:3:1 is in agreement with there being three equivalent F nuclei. The second feature is the much less resolved structure centered at 3570 G, which arises from the x,y part of the g tensor and fluorine A tensors. The x,y block of the g tensor is diagonal, and the lines are centered around $g_{\perp}$(=g_{zz} = g_{yy}). The line pattern has been interpreted in terms of a diagonal x,y part of the fluorine A tensors, with $A_{xx} = A_{yy} = A_{\perp}$, the $A_{\perp}^{\text{F}}$ being estimated at ca. 10.3−11.5 MHz (depending on the rare gas matrix). The main Ti isotope, ^{48}Ti, has zero spin and only two Ti isotopes, with abundances of only 7% and 5%,

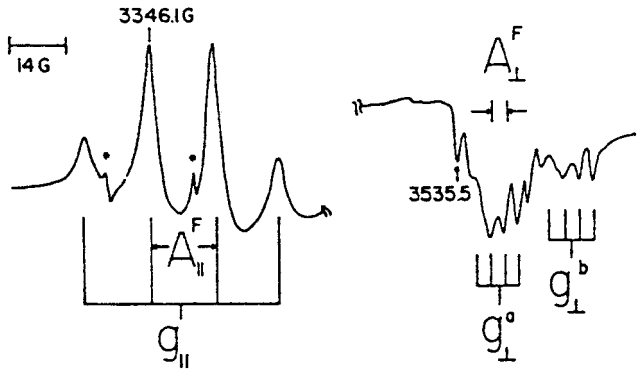

Figure 1. Experimental ESR spectrum from ref 2. To the left, the "parallel" lines centered around 3350 G are shown; to the right, "perpendicular" lines centered at 3550 G are shown. Note that there is assumed to be a second less occupied site b in the matrix, leading to the set of lines with g value $g_{\perp}^{b}$.

have nonzero spin. From the accordingly weak lines caused by the Ti hyperfine splitting, the Ti A tensor has been deduced, which has been discussed in our previous paper. We will not discuss it here.

Figure 3 of ref 2 gives both the fluorine hyperfine splitting patterns on an enlarged horizontal scale and is reproduced here in Figure 1, since we will often refer to it in the following discussion. It is believed that there is, apart from the mainly populated a site in the matrix, also a b site in the neon lattice, giving rise to a slightly shifted set of lines (around $g_{\perp}^{b}$). A simulation of the spectrum with the CWR program, employing the parameters of ref 2 for the Ar matrix ($g_{\perp} = 1.8786$, $g_{||} = 1.9986$, $A_{\perp}^{F} = 10.3$ MHz, $A_{||}^{F} = 44.7$ MHz) is shown in Figure 2a. Of course, the position and line pattern of the parallel part to the left (around 0.335 T), being determined by $g_{||}$ and $A_{||}^{F}$, agrees with the experimental one (cf. also Figure 2 of ref 2). The perpendicular part has roughly the same shape as the experimental one (see in particular Figure 2 of ref 2), but there is not detailed agreement when one considers the peak structures in Figure 2a and Figure 1 (note that the intensities of the parallel and perpendicular parts have obviously been scaled differently in Figure 1). Obviously, other choices for the x,y part of the fluorine A tensor might yield similar agreement with experiment. However, the calculated parameters in Table 1 can definitely be ruled out as reasonable alternatives. In Figure 2b the parameters according to the spin-restricted calculations ($A_{xx}^{F} = 17.9$ MHz, $A_{yy}^{F} = 59.3$ MHz, $A_{zz}^{F} = 15.8$ MHz) have been used. Note that these A tensor principal values refer to F atom number 1, which is located at the x-axis; the A tensors on the other F nuclei are of course suitably transformed. Clearly, $A_{zz}^{F} = 15.8$ is too small, whereas the perpendicular components are too large, the perpendicular part of the spectrum becomes too wide and has a wrong peak structure. Similarly, the spin-unrestricted results of Table 1, which yield the spectrum of Figure 2c, are not correct, in particular $A_{zz}^{F} = 80.9$ MHz is much too large. The perpendicular part seems to be too wide, but the peak structure is reasonable, a point that will be considered in more detail later.

We will now first consider which approximations or deficiencies in the theoretical treatment, or assumptions in the experimental assignment, may be held responsible for the lack of agreement between theory and experiment. First, the traceless part of the fluorine A tensor, arising from the dipolar operator, will be discussed, and next the contact part.

Dipolar Contribution to the Fluorine A Tensor. A_{dip} will have significant contributions from the unpaired spin orbital and from spin polarization effects in lower lying fully occupied orbitals. In Table 4 the energies and compositions of the valence and subvalence orbitals are displayed. The unpaired spin-orbital, $7a_1'\uparrow$ has predominantly 3d character (71%), a sizable amount

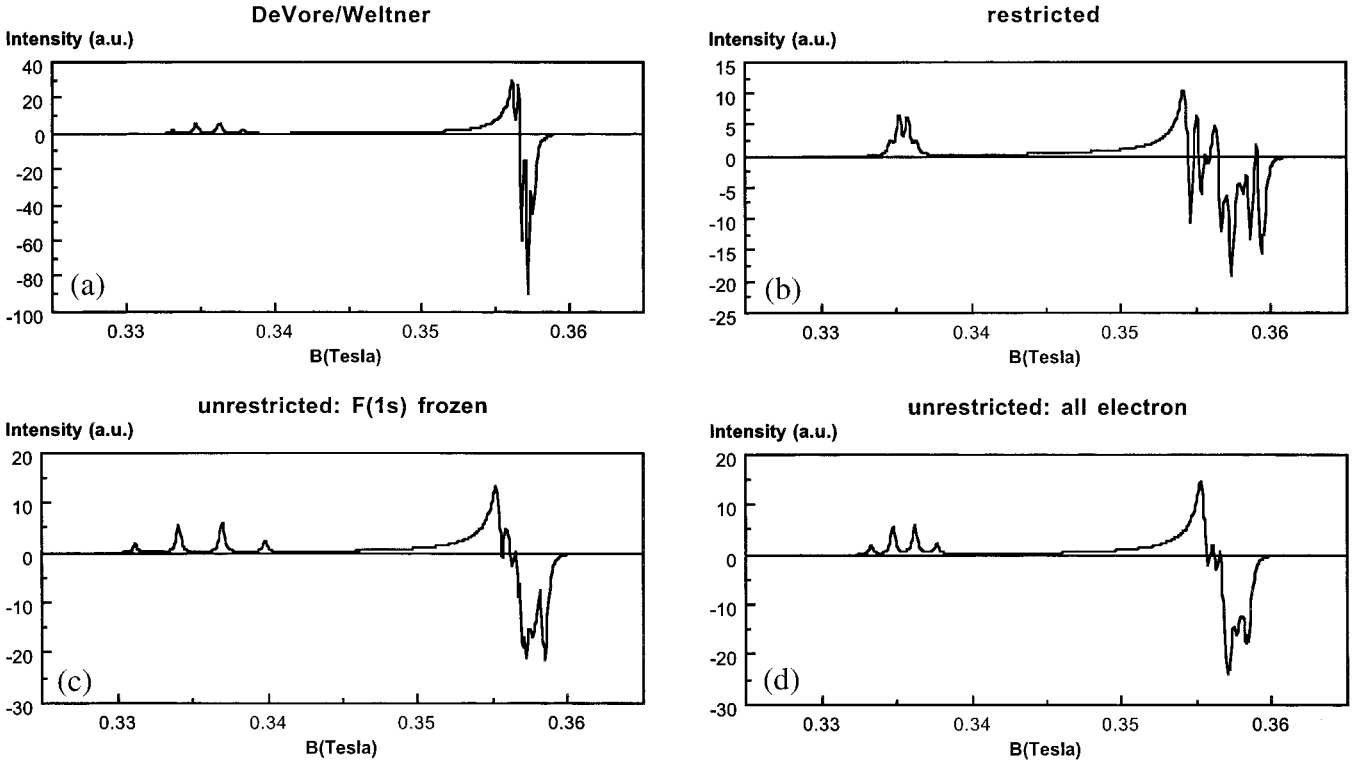

Figure 2. Simulated ESR spectra of TiF_3 using the following choices for the principal A tensor values at F: (a) experimental A tensors of De Vore and Weltner,[2] $A_{zz} = 44.7$ MHz, $A_{xx} = A_{yy} = 10.3$ MHz; (b) A tensors from the spin-restricted calculations, Table 1, $A_{zz} = 15.8$ MHz, $A_{xx} = 17.9$ MHz, $A_{yy} = 59.3$ MHz; (c) A tensors from the spin-unrestricted calculations, frozen F 1s core, Table 1, $A_{zz} = -80.9$ MHz, $A_{xx} = -34.5$ MHz, $A_{yy} = -12.7$ MHz; (d) A tensors from the spin-unrestricted calculations, no frozen core, Table 6, $A_{zz} = -40.7$ MHz, $A_{xx} = 33.7$ MHz, $A_{yy} = 11.2$ MHz.

TABLE 4. One-Electron Eigenfunctions and Eigenvalues for the Unrestricted Calculation[a]

	orbital	energy (eV)	description (%)
Ti 3d	$2e_1''\downarrow$	−3.86	88.11 Ti($3d_{xz,yz}$) + 10.44 F($2p_{\pi,\perp}$)
	$2e_1''\uparrow$	−4.33	86.59 Ti($3d_{xz,yz}$) + 12.15 F($2p_{\pi,\perp}$)
	$7a_1'\downarrow$ (LUMO)	−4.07	28.77 Ti(4s) + 68.67 Ti($3d_{z^2}$) + 2.26 F($2p_\sigma$)
	$7a_1'\uparrow$ (HOMO)	−5.35	24.35 Ti(4s) + 71.37 Ti($3d_{z^2}$) + 3.29 F($2p_\sigma$)
F 2p	$1a_2''\uparrow$	−10.32	100.00 F($2p_\pi^{ip}$)
	$1a_2'\downarrow$	−10.35	100.00 F($2p_\pi^{ip}$)
	$6e_1'\uparrow$	−10.57	0.70 Ti($3p_{x,y}$) + 1.06 Ti($4p_{x,y}$) + 36.64 F($2p_\sigma$) + 60.32 F($2p_\pi^{ip}$)
	$6e_1'\downarrow$	−10.58	0.76 Ti($3p_{x,y}$) + 0.91 Ti($4p_{x,y}$) + 37.43 F($2p_\sigma$) + 59.70 F($2p_\pi^{ip}$)
	$3a_2''\uparrow$	−10.68	2.97 Ti($4p_z$) + 96.56 F($2p_{\pi,\perp}$)
	$3a_2''\downarrow$	−10.68	2.28 Ti($4p_z$) + 97.27 F($2p_{\pi,\perp}$)
	$1e_1''\downarrow$	−11.05	10.24 Ti($3d_{xz,yz}$) + 89.83 F($2p_{\pi,\perp}$)
	$1e_1''\uparrow$	−11.07	11.96 Ti($3d_{xz,yz}$) + 88.00 F($2p_{\pi,\perp}$)
	$6a_1''\downarrow$	−11.63	0.35 Ti(3s) + 0.54 Ti(4s) + 5.76 Ti($3d_{z^2}$) + 1.57 F(2s) + 90.24 F($2p_\sigma$)
	$6a_1'\uparrow$	−11.69	0.30 Ti(3s) + 0.52 Ti(4s) + 7.29 Ti($3d_{z^2}$) + 1.66 F(2s) + 88.55 F($2p_\sigma$)
	$5e_1'\downarrow$	−11.77	0.37 Ti($3p_{x,y}$) + 0.41 Ti($4p_{x,y}$) + 17.20 Ti($3d_{x^2-y^2,x,y}$) + 0.97 F(2s) + 49.43 F($2p_\sigma$) + 31.34 F($2p_\pi^{ip}$)
	$5e_1'\uparrow$	−11.83	0.35 Ti($3p_{x,y}$) + 0.41 Ti($4p_{x,y}$) + 18.58 Ti($3d_{x^2-y^2,x,y}$) + 1.03 F(2s) + 49.29 F($2p_\sigma$) + 30.00 F($2p_\pi^{ip}$)
F 2s	$4e_1'\downarrow$	−28.48	4.69 Ti($3p_{x,y}$) + 1.21 Ti($3d_{x^2-y^2,xy}$) + 96.66 F(2s) + 0.07 F($2p_\sigma$)
	$4e_1'\uparrow$	−28.48	4.23 Ti($3p_{x,y}$) + 1.28 Ti($3d_{x^2-y^2,xy}$) + 96.97 F(2s) + 0.09 F($2p_\sigma$)
	$5a_1'\uparrow$	−29.00	0.38 Ti(3s) + 0.87 Ti($3d_{z^2}$) + 99.79 F(2s) + 0.88 F($2p_\sigma$)
	$5a_1'\downarrow$	−29.02	0.42 Ti(3s) + 0.79 Ti($3d_{z^2}$) + 99.9 F(2s) + 0.87 F($2p_\sigma$)
Ti 3p	$2a_2''$	−38.57	99.73 Ti($3p_z$) + 0.15 F($2p_{\pi,\perp}$)
	$2a_2''\uparrow$	−39.48	99.80 Ti($3p_z$) + 0.13 F($2p_{\pi,\perp}$)
	$3e_1'\downarrow$	−39.58	94.01 Ti($3p_{x,y}$) + 4.28 F(2s) + 1.41 F($2p_\sigma$)
	$3e_1'\uparrow$	−40.07	94.58 Ti($3p_{x,y}$) + 3.83 F(2s) + 1.33 F($2p_\sigma$)
Ti 3s	$4a_1'\downarrow$	−61.80	98.94 Ti(3s) + 0.32 F(2s) + 0.46 F($2p_\sigma$)
	$4a_1'\uparrow$	−62.45	98.97 Ti(3s) + 0.31 F(2s) + 0.45 F($2p_\sigma$)

[a] The DZ (1s frozen) basis set was employed (for a description see Table 2). ⊥ = perpendicular to *xy*-plane; ip = in-plane.

of 4s character (24%), and a small amount (3.3%) of F $2p_\sigma$ character that is crucial for the present discussion. Below this level there is the fully occupied set (18 electrons) of nominally F 2p orbitals, in a small energy range of −10.3 to −11.8 eV. The polarization of these in response to the small amount of $2p_\sigma$ unpaired electron will be detailed below. The lower lying, energetically well separated sets of F 2s, Ti 3p, and Ti 3s levels will play a role in the discussion of the contact term later.

In Table 5 the polarization in the 2p shell is reported by giving the *A* tensor components per orbital. Only the first-order contributions to the dipolar term of the *A* tensor are reported, since the second-order ones are negligible (see Table 1), and only the one-center contributions are shown per orbital. The two-center contributions, stemming mostly from the unpaired spin orbital, are given separately.

We first comment on the spin-restricted results, with an unpaired electron in $7a_1'$ and no spin polarization in occupied shells. The dipolar part of the *A* tensor on F is small, in agreement with the small participation of the fluorine 2p orbitals in the MO containing the unpaired electron, and, as long as we do not include the first order, two-center contributions, is close to axial symmetry along the Ti−F bond. The pattern of an A_{bond} value that is twice as large and has opposite sign to the other two principal values is typical for a 2p (in this case $2p_\sigma$) spin density. However, if we take into account the two-center contributions to the first-order *A* tensor, this axial symmetry of the coupling tensor, along the bond, is destroyed. We have analyzed in greater detail the two-center term Ti−F−Ti (dipolar operator on F, functions on Ti), splitting it up into individual contributions. The largest contribution is observed when both functions on titanium are 3d orbitals, i.e., from the term ⟨3d F 3d⟩ (18.3 MHz). This value is somewhat counteracted by the ⟨3s F 4s⟩ (−2.2 MHz) and ⟨4s F 3d⟩ (−3.2 MHz) terms. The total Ti−F−Ti contribution along the bond is 17.2 MHz. For the other two directions of the *A* tensor, the ⟨3d F 3d⟩ term gives smaller contributions, −8.2 MHz and −10.1 MHz for normal to the bond and along the *z*-axis, respectively. The total Ti−F−Ti contributions normal to the bond and along the *z*-axis are −10.3 and −6.9, respectively. Clearly, the two-center

TABLE 5. Individual Contributions to the A_{dip} Term (First Order)[a]

	A_{dip} (first order)		
	along bond A_{bond}	normal to bond $A_\perp$	along *z*-axis A_{zz}
	Restricted		
$7a_1'$ (1-center contr.)	18.7	−9.2	−9.5
2-center contr.	14.8	−9.2	−5.4
total	33.5	−18.4	−14.9
	Unrestricted		
$7a_1'$ (Ti $3d_{z^2}$,4s) (α)	22.9	−11.3	−11.5
	F 2p Polarization		
$6a_1'$(F $2p_\sigma$) Δ(α−β)	−17.1	8.5	8.5
$5e_1'$(F^1 $2p_\sigma$) Δ(α−β)(1)	−5.9	3.0	2.9
$6e_1'$(F^1 $2p_\sigma$) Δ(α−β)(1)	−16.5	8.3	8.2
$2p_\sigma$ total	−39.5	19.8	19.6
a_2'(F $2p_\pi^{ip}$) Δ(α−β)total	0.9	−1.6	0.9
$5e_1'$(F^1 $2p_\pi^{ip}$) Δ(α−β)(2)	12.2	−24.3	12.2
$6e_1'$(F^1 $2p_\pi^{ip}$) Δ(α−β)(2)	−4.0	7.9	−4.0
$2p_\pi^{ip}$ total	9.1	−18.0	9.1
a_2''(F $2p_z$) Δ(α−β)total	5.1	5.1	−10.1
e_1''(F $2p_z$) Δ(α−β)total	19.7	19.7	−39.5
$2p_{\pi,\perp}$ total	24.8	24.8	−49.6
total 1-center	16.9	15.3	−32.2
2-center	16.7	−10.9	−5.9
total	33.6	4.4	−38.1

[a] The restricted and unrestricted cases are considered, using the DZ (1s frozen) basis set described in Table 2. F^1 denotes the fluorine atom whose bond with Ti lies along the *x*-axis. The *A* tensor on this atom is calculated. The most important contributions to A_{dip} in each symmetry are also shown. The $2p_\sigma$ AO on F^1 ($2p_x^1$) only occurs in component (1) of E_1' symmetry. The $2p_\pi^{ip}$ AO on F^1 ($2p_y^1$) occurs only in component (2) of E_1' symmetry. Therefore, the *A* tensor for F^1 exhibits only $2p_\sigma$ polarization in e_1'(1) orbitals, and only $2p_\pi^{ip}$ polarization in e_1'(2) orbitals.

TABLE 6. Effect of the F Basis Set on *A* Values for TiF_3 (Unrestricted)[a]

	A_{dip} (first order)[c]			A_{dip} (total, traceless)[c]			$A_{contact}$[b]		
basis set	along bond (F)	normal to bond (F)	along *z*-axis (F)	along bond (F)	normal to bond (F)	along *z*-axis (F)	(from all functions)	(from functions on nucleus)	A_{iso}
DZ 1s frozen	33.6	4.4	−38.1	30.0	8.2	−38.2	−44.6	−44.1	−42.7
TZ 1s frozen	36.9	5.2	−42.0	32.5	9.7	−42.2	−43.6	−41.0	−41.3
all electrons[B]	37.3	5.6	−43.0	33.0	10.1	−43.2	11.5	15.2	13.8
all electrons[C]	36.3	5.6	−41.9	32.2	9.8	−42.1	−4.1	−4.2	−1.9
all electrons[D]	36.3	5.6	−41.9	32.2	9.9	−42.1	−3.7	−3.9	−1.5
all electrons[E]	36.4	5.6	−42.0	32.3	9.8	−42.1	−0.8	−2.1	1.4
all electrons[F]	37.3	5.6	−41.9	32.2	9.8	−42.0	−6.3	−6.3	−4.1
all electrons[G]	37.2	6.4	−43.6	33.1	10.8	−43.8	−0.2	−1.0	1.9

[a] All *A* tensor values are expressed in MHz. For a brief description of the basis sets see Table 3. For Ti the all-electron basis set ae^B is used. [b] The contact term is split into a set of results obtained simply by one-center contributions $1s^k \cdot 1s^k$ from functions on nucleus k = F), and a set obtained including also the off-center contributions $1s^k \cdot \chi_\mu^{k'}$ (from all functions). [c] The following calculated *A* values represent the first order term and the sum of the first- and the second-order terms (total, traceless) (eq 2), without the Fermi contact contribution and without the isotropic "pseudocontact" contribution that arises from the second-order terms in the *A* tensor expression. The latter are given separately ($A_{contact}$ and $A_{iso} = A_{contact} + A_{pseudocontact}$, respectively).

integrals in which the dipolar operator has its origin on fluorine, while both basis functions have their origin on titanium, give by far the largest contribution. This is not surprising, as about 90% of the MO containing the unpaired electron is localized on titanium. With such an off-center (with respect to F) distribution of the unpaired electron, the two-center contribution is comparable to the one-center contribution. One obviously cannot relate the full tensor any more to the on-site character of the unpaired electron. The two-center terms change the along-bond character of the *A* tensor based on one-center contributions only but do not convert it to along-*z*-axis axial character. The spin-restricted results are not in agreement with experiment in this respect, and surely the total A_{zz} is too small.

The unrestricted results for the dipolar part are qualitatively different. The $7a_1'\uparrow$ orbital does not change much and so its contribution to the *A* tensor stays pretty much the same. This holds for the one-center contributions and for the two-center contributions, given separately at the bottom of the table, as well, in agreement with the latter being determined by the unpaired electron orbital. However, the spin polarization effects in the 2p shell are quite significant. We find $2p_\sigma$ character on fluorine atom nr. 1 (the fluorine atom along the *x*-axis, for which the *A* tensor is evaluated) in orbitals in a_1' symmetry and in component 1 of e_1' symmetry. Although the differences between the up-spin and down-spin orbitals, as given in Table 4, are only small, they are large enough to lead to significant polarization effects as compared to the "zero-order" *A* tensor coming from the $7a_1'\uparrow$ orbital. Of course the polarization of $2p_\sigma$-containing orbitals does not destroy the along-bond axial character of the $7a_1'\uparrow$ *A* tensor, but it is destroyed by the polarization of the $2p_\pi^{ip}$ (in-plane, perpendicular to the bond, i.e., $2p_y$ on F^1) and the $2p_z$, having their main axes in different directions. The polarization contributions of these 2p orbitals are again considerable. As we can infer from Table 5, the net result of the spin polarization of the 2p shells in our particular case is an entirely fortuitous axial symmetry, in the direction of the *z* -axis, for the total one-center contribution. This *z*-axial character of the *A* tensor is then again removed by the strong effect of the two-center terms.

The net result is a dipolar *A* tensor with comparable principal values along the *z*-axis and along the Ti−F bond, with opposite signs, however, and a small principal value in the plane normal to the bond.

In Table 6 some tests of the dependence of these results on the basis set and on the frozen core approximation are given. The DZ basis, with frozen F 1s core and Ti 1s−2p core, used until now has been replaced (see Table 2) by a TZ basis keeping the same core shells frozen, next all cores have been unfrozen while keeping the same TZ valence basis (all-electron basis B), while subsequently the core and valence basis sets have been extended (all electron basis sets C−G). When we first consider the first-order dipolar *A* tensor, it is clear from Table 6 that there is a small effect from the extension of the valence basis from DZ to TZ, which is due to the fact that the very negatively charged F ions need a somewhat better than DZ basis. After that point, the basis set effects are minor. The same holds true for the traceless *A* tensor with second-order contributions included (Table 6 second column). The second-order contributions increase the normal-to-bond component A_{yy} somewhat.

Fermi Contact Contribution to the Fluorine A Tensor. We have already noted a change of sign and magnitude in the contact term, from +28.1 to −44.6 MHz, on passing from the restricted to the unrestricted case (see Table 1). In these calculations, the F 1s core was still frozen, and therefore the results of Table 1 probably reflect primarily spin polarization of the 2s AO. The $A_{contact}$ values may also be sensitive to unfreezing the 1s core. In Table 6 the effect of unfreezing the F 1s core on $A_{contact}$ is made visible. We note first that changing the valence basis set from DZ to TZ while keeping 1s frozen has very little effect on $A_{contact}$. Unfreezing the 1s, however, affects $A_{contact}$ strongly. This term settles (apart from the "special" value obtained with the basis set of type B) to a value in the range −4.1 to −0.2 MHz with all the other "all-electrons" basis sets. The basis set B has only a DZ representation of the 1s core. This is apparently not sufficient, or the exponents should be optimized, but TZ or beyond will do. In the last column of Table 6, the total isotropic part of the *A* tensor is given, which includes the isotropic contribution from the dipolar operator in second order. This contribution is apparently small.

In Table 7 the effect of spin polarization contributions from various shells on the Fermi contact term is presented. Only the results obtained simply by one-center contributions (from functions on fluorine nucleus) are reported, because the off-center contributions (from all functions) are negligible, as we can see from Table 6. The data for F 1s frozen are given both for the restricted and unrestricted cases. The basis set is the DZ basis on F, with F 1s frozen, and the TZ basis on Ti, with 1s−2p frozen. This basis has been used for Table 1 and Table 4 as well. The all-electron calculation used the all-electron basis set ae^C for F and ae^B for Ti, as described in Table 2.

We discuss first the results with F 1s frozen. In the spin-restricted calculation there is only the +24.6 MHz contribution

TABLE 7. Contributions to the $A_{contact}$ Term (from Functions on Fluorine Nucleus) for the Restricted and Unrestricted Cases

	F 1s frozen[b]			all electrons[a]		
	$\rho(0)$ (au)	$\rho^{\uparrow}(0)-\rho^{\downarrow}(0)$ (au)	$A_{contact}$ (MHz)	$\rho(0)$ (au)	$\rho^{\uparrow}(0)-\rho^{\downarrow}(0)$ (au)	$A_{contact}$ (MHz)
			Restricted			
$7a_1'$	0.0058		+24.6			
			Unrestricted			
$7a_1'(\text{Ti } 3d_{z^2},4s)^{\uparrow}$	0.0048	+0.0048	+20.1	0.0043	+0.0043	+18.1
$3e_1'(\text{Ti } 3p_{x,y})^{\uparrow}$	0.2573			0.2194		
$3e_1'(\text{Ti } 3p_{x,y})^{\downarrow}$	0.2880	−0.0307	−129.3	0.2458	−0.0264	−110.9
$4a_1'(\text{Ti } 3s)^{\uparrow}$	0.0041			0.0036		
$4a_1'(\text{Ti } 3s)^{\downarrow}$	0.0044	−0.0003	−1.4	0.0039	−0.0003	−1.2
$2e_1'(\text{Ti } 2p_{x,y})^{\uparrow}$				0.0000		
$2e_1'(\text{Ti } 2p_{x,y})^{\downarrow}$				0.0000	0.0000	small
$3a_1'(\text{Ti } 2s)^{\uparrow}$				0.0000		
$3a_1'(\text{Ti } 2s)^{\downarrow}$				0.0000	0.0000	small
$1a_1'(\text{Ti } 1s)^{\uparrow}$				0.0000		
$1a_1'(\text{Ti } 1s)^{\downarrow}$				0.0000	0.0000	small
$6e_1'(\text{F } 2p_{\sigma},2p_{\pi}^{ip})^{\uparrow}$	0.0195			0.0163		
$6e_1'(\text{F } 2p_{\sigma},2p_{\pi}^{ip})^{\downarrow}$	0.0191	+0.0004	+1.7	0.0158	+0.0005	+2.0
$6a_1'(\text{F } 2p_{\sigma})^{\uparrow}$	0.0829			0.0707		
$6a_1'(\text{F } 2p_{\sigma})^{\downarrow}$	0.0786	+0.0043	+18.1	0.0667	+0.0040	+17.0
$5e_1'(\text{F } 2p_{\sigma},2p_{\pi}^{ip})^{\uparrow}$	0.0774			0.0657		
$5e_1'(\text{F } 2p_{\sigma},2p_{\pi}^{ip})^{\downarrow}$	0.0720	+0.0054	+22.8	0.0608	+0.0050	+21.0
$5a_1'(\text{F } 2s)^{\uparrow}$	4.2963			3.7002		
$5a_1'(\text{F } 2s)^{\downarrow}$	4.3058	−0.0095	−39.8	3.7085	−0.0083	−35.1
$4e_1'(\text{F } 2s)^{\uparrow}$	8.4576			7.3129		
$4e_1'(\text{F } 2s)^{\downarrow}$	8.4424	+0.0151	+63.7	7.3004	+0.0125	+52.5
$2a_1'(\text{F } 1s)^{\uparrow}$				70.1713		
$2a_1'(\text{F } 1s)^{\downarrow}$				70.1688	+0.0026	+10.8
$1e_1'(\text{F } 1s)^{\uparrow}$				140.3419		
$1e_1'(\text{F } 1s)^{\downarrow}$				140.3368	+0.0051	+21.4
total			−44.1			−4.2

[a] The all-electron basis sets ae^C for F and ae^B for Ti described in Table 2 are used. [b] The DZ 1s frozen for F and the TZ 1s−2p frozen for Ti basis sets described in Table 2 are used.

from the $7a_1'$, coming from the very small percentage of F 2s character of the unpaired spin orbital. When the calculation is carried out spin unrestricted, the contribution of the $7a_1'$ does not change much (+20.1 MHz). However, there are much larger effects from spin polarization of the 2s shell, which manifests itself in slightly different 2s contributions to corresponding up and down spin levels, cf. Table 4. The F 2s mixes slightly with the Ti 3p, and as a consequence the largest contributions are coming from the (nominally) Ti 3p levels $3e_1'$ (−129.3 MHz) and the (nominally) F 2s levels $4e_1'$ (+63.7) and $5a_1'$ (−39.8). Note that, for instance in the $5a_1'$ orbital, which is mostly F 2s, a 0.1% difference in 2s content of $5a_1'^{\uparrow}$ and $5a_1'^{\downarrow}$ is sufficient to cause this spin polarization. The nominally F 2p levels $5e_1'$ and $6a_1'$ have little F 2s character (cf. the small $\rho(0)$ values compared to the F 2s orbitals), but the differences between the up and down spin−orbitals are still sufficient to make a contribution to the spin polarization (+22.8 and +18.1 MHz, respectively). We thus see that the reversal of the positive Fermi contact term of +24.6 MHz for the restricted calculation (+28.1 MHz if also off-center functions are included, see Table 1) to −44.1 MHz in the unrestricted calculation is indeed fully caused by F 2s spin polarization. The effect of unfreezing the F 1s (and the change to a larger basis set) can be observed to have a fairly small effect on the individual orbital contributions (right panel in Table 7). The total 2s polarization (from $3e_1'$, $4e_1'$, $5a_1'$, $5e_1'$, and $6a_1'$) stays approximately the same, dropping slightly from −64.2 MHz to −54.7 MHz. However, the F 1s core spin polarization effect (levels $1e_1'$, $2a_1'$) is significant, +32.2 MHz. Taken together with the ca. +10 MHz effect of the reduction in 2s polarization, unfreezing the F 1s reduces the contact term to almost zero (−4.2 MHz in the present basis ae^C, −1.0 MHz (from functions on the F nucleus only) in the case of the largest basis ae^G, cf. Table 6).

We conclude that spin polarization of the 1s and 2s shells makes the difference between the restricted and unrestricted $A_{contact}$ values and taking them both into account is essential for a correct determination of the contact term of the fluorine hyperfine coupling. The opposite polarizations of inner shells and their relatively large contributions to the contact term have been noted and discussed before.[1,44,45]

Comparison to Experiment. Considering that the total *A* tensor is determined by both contact and dipolar parts, we clearly understand the importance of the 1s spin polarization. When the 1s shell is frozen, the A_{zz} total component of the *A* tensor is given by the sum $-38.2 - 42.7 = -80.9$ MHz (see Table 6, basis set DZ 1s frozen), i.e., the contact and dipolar parts contribute to roughly the same extent. We have noted above that this value of the A_{zz} is definitely too large compared to the experimental value of 44.7 MHz (in Ar matrix). When the 1s shell is unfrozen, the sum modifies in $-43.8 + 1.9 = -41.9$ MHz (see Table 6, basis set all electrons[G]), and the total *A* tensor turns out to be determined in practice only by the dipolar part, which has already been discussed. To compare our results with experiment, we run a simulation with the principal values of the *A* tensor as determined now (see Table 6, all electron basis set E), i.e., $A_{zz} = 40.7$ MHz, $A_{xx} = 33.7$ MHz, and $A_{yy} = 11.2$ MHz. This simulation is shown in Figure 2d. The parallel part is in excellent agreement with experiment. The perpendicular part appears to be too wide, indicating that the *xx* and *yy* principle values of the *A* tensor are too large. However, the peak structure is reasonable. Counting the minima starting from the left, we encounter first a pronounced minimum, corresponding

TABLE 8. Theoretical Magnetic Proton *A* Parameters for CH_3 in the Local Density Approximation (LSD)[b]

	A tensor at H		
	along bond (H)	normal to bond (H)	along *z*-axis (H)
DZ 1s Frozen			
1-center	−0.3	−0.4	0.7
2-center C−H−H	−0.9	−1.3	2.2
2-center C−H−C	28.9	−35.0	6.0
2-center total	28.0	−36.3	8.3
A total (traceless)	27.7	−36.7	8.9
A_{Fermi} (from functions on nucleus)		−77.5	
A_{Fermi} (from all functions)		−60.8	
A_{iso}		−60.8	
All Electrons[A]			
1-center	−3.0	−0.5	3.5
2-center C−H−H	−0.7	−1.7	2.4
2-center C−H−C	28.2	−35.4	7.1
2-center total	27.5	−37.1	9.5
A total (traceless)	24.5	−37.5	13.0
A_{Fermi} (from functions on nucleus)		−85.3	
A_{Fermi} (from all functions)		−53.9	
A_{iso}		−53.9	
Experimental[a]			
A_{iso}		−64.5	
A_{dip}	35.1	−35.1	1.4−2.2

[a] From refs 24 and 47. [b] All *A* tensor values are expressed in MHz. The first-order contributions are split in one- and two-center contributions. Second-order contributions are negligible. For a basis set description see Table 3.

to the one at 3535.5 G in the experimental spectrum, then a small one that is discernible as a shoulder in the experimental spectrum, then a shoulder that is not visible in the experimental spectrum, and finally three minima that correspond to minima in the experimental spectrum (note that the remaining peaks in the experimental spectrum can be ascribed to the b sites; both at the a and the b sites we assign a leftmost peak that is not assigned in ref 2). We conclude that the calculated A_{zz} tensor component is in excellent agreement with experiment, while the principal values of the *A* tensor that give rise to the "perpendicular part" of the spectrum appear to have a good ratio, but their absolute values are somewhat too large.

It should be noted that the calculated A_{zz} has opposite sign to A_{xx} and A_{yy}. In the experimental work, the signs are not determined and they have been assumed equal. It would be justified, in view of our results, to recalculate the "experimental" A_{iso} by taking the sign for the $A_\perp$ (keeping the single value 10.3 or 11.5 MHz for $A_{xx} = A_{yy} = A_\perp$) oppposite to that of A_{zz}. The experimental A_{iso} then becomes considerably smaller than the 23.6 MHz quoted in Table 1, namely 8.3−8.0 MHz, depending on the matrix. This correction of the experimental number improves the agreement with the calculations.

3.2. The CH_3 Radical. We will briefly consider the CH_3 radical, since it is a prototype organic radical sufficiently analogous to and at the same time sufficiently different from the TiF_3 radical to make a comparison useful. The hyperfine structure has been extensively studied theoretically.[5,9,11−17] We will study in more detail the mechanism of the hyperfine splitting and the relative importance of various contributions. CH_3 is a $(2p_z)^1$ radical, while TiF_3 is a $(3d_{z^2})^1$ radical. The H isotropic hyperfine splitting has to derive, at least in the D_{3h} equilibrium structure, from spin polarization. This holds for the isotropic hfsc of F in TiF_3 too, if we start from the zero-order $2p_\sigma$ spin density, but the mechanism of spin polarization is somewhat different, see the Discussion.

Table 8 lists the *A* tensor values for hydrogen in CH_3 for two different basis sets, using spin-unrestricted LDA (LSD) calculations. The DZ set, with 1s on C frozen, and the all-electron (no frozen 1s on C) TZ basis set denoted ae^A are described in Table 3. Our calculations estimate that the single π electron in carbon induces a negative spin density of about −0.055 electrons in the hydrogen 1s orbital. This leads to a Fermi contact hyperfine splitting of −77.5 to −85.3 MHz (cf. A_{Fermi} from functions on the nucleus). There are sizable corrections in this case coming from spin density described by other functions, such as 2s and $2p_\sigma$ on C, yielding final isotropic hyperfine splitting constants of −54 to −61 MHz. This is in rather good agreement with observed proton splittings in the methyl radical (−64.5 MHz[24]), although vibrational averaging effects would lower the calculated values by some 5 MHz.[15] There are no isotropic pseudocontact contributions from second-order effects of the dipolar operator.

The dipolar contributions to the *A* tensor are expected to be quite small inasmuch as they are coming from spin density at the H atom, in view of the predominantly s-like nature of the unpaired spin density at H. Indeed, very small values are obtained from the one-center terms, arising from the presence of a very small negative spin density in the hydrogen $2p_\sigma$ orbital, resulting from the spin polarization of the C−H bonding electrons (see the Discussion). However, more significant contributions come from two-center terms, due to the large spin density in the C $2p_z$ orbital. It is clear from Table 8 that those two-center terms dominate that have the operator at H and both basis functions located at C. Such terms are not very sensitive to the basis set, since they do not arise from details in the spin density distribution, but just from its C $2p_z$ character. Comparison with experiment shows good agreement for the largest component, the one in the molecular plane normal to the C−H bond. The component along the C−H bond is also large, although not as large as the experimental one, which is equal to the perpendicular in-plane component. The experimental *zz* component is negligible, but the calculated one is not, although it is considerably smaller than the other components. We note that both an ab initio[12] and a DFT[5] calculation report a small component perpendicular to the plane. We have therefore repeated the calculation with a very large STO basis set (on H, QZ 1s, DZ 2p,3d; on C, TZ 1s, QZ 2s,2p, DZ 3d.4f) but did not observe a significant change with respect to the ae^H basis set, in agreement with the observed dominance of the two-center terms which are not expected to be very sensitive to basis set quality. The overall agreement may still be considered fair, in particular since vibrational averaging is not taken into account.

3.3. Effect of Density Functionals with Gradient Corrections. Investigations on small organic radicals[5,8,9] pointed out that the inclusion of the density gradient corrections (generalized gradient approximations, GGA) gives an important improvement over the local spin density approximation (LSD). Particularly the gradient exchange correction scheme by Perdew and Wang,[37] has been recommended as leading to Fermi contact terms in very good agreement with experiment. In this section we will deal with the effects of various gradient corrections to the exchange and correlation potentials on the hf structure of CH_3 and TiF_3. Also the hyperfine splittings due to the central nuclei, C and Ti, are now considered.

Table 9 lists the unrestricted *A* tensor values of the organic radical, obtained using the different DFT functional forms indicated and previously described and, in each case, using the optimized geometry and the most extensive all-electron basis set with superscript "H" (see Table 3 for a description). The experimental isotropic and anisotropic *A* tensor values are also

TABLE 9. Isotropic and Anisotropic Hyperfine *A* Tensors (in MHz) of the CH_3 Radical, Obtained Using the Different DFT Functional Forms Indicated[c]

			A_{dip} (total,traceless)		
functional form	nucleus	A_{iso}	along bond	normal to bond	along *z*-axis
LSD	^{13}C	45.9	−78.9	−78.9	157.7
	^{1}H	−53.9	24.5	−37.5	13.0
BP	^{13}C	81.8	−81.2	−81.2	162.4
	^{1}H	−67.0	22.7	−37.9	15.1
PW91	^{13}C	73.9	−81.2	−81.2	162.5
	^{1}H	−61.5	22.4	−37.5	15.1
PW86	^{13}C	76.7	−81.8	−81.8	163.6
	^{1}H	−59.0	21.7	−37.2	15.5
EXP[a]	^{13}C	108.0−105.6	−62.2 to 63.6	−62.2 to −63.6	128.3−124.0
	^{1}H	−64.6 to −62.5	35.1	−35.1	1.4−2.2
EXP[b]	^{13}C	75.6			
	^{1}H	−70.0			

[a] Direct experimental results from refs 24 and 47. [b] These experimental results correspond to the hypothetical nonvibrating planar molecule from refs 15, 16 and 18. [c] The optimized geometry and the all electron basis set ae^H were used throughout (see Table 3).

TABLE 10. Hyperfine *A* Tensor (in MHz) of TiF_3, Obtained Using the Different DFT Functional Forms As Listed[b]

	fluorine atom, ^{19}F				
		A_{dip} (total,traceless)			
functional form	A_{iso}	along bond (F)	normal to bond (F)	along *z*-axis (F)	titanium atom, ^{47}Ti A_{iso}
		Basis Sets ae^F on F and ae^B on Ti			
LSD	−4.1	32.2	9.8	−42.0	−245.9
BP	+0.1	29.0	9.8	−38.8	−233.0
PW91	+0.8	26.0	5.5	−31.5	−233.4
PW86	+7.2	20.8	5.8	−26.6	−238.9
		Basis Sets ae^G on F and ae^B on Ti			
LSD	+1.9	33.1	10.8	−43.8	
BP	+7.1	29.5	10.7	−40.3	
PW91	+5.7	26.7	6.5	−33.1	
PW86	+10.9	21.0	6.3	−27.4	
EXP[a]	8.3−8.0				−184.8 to −177.1

[a] Experimental values from ref 2, with correction for a different sign of perpendicular and parallel principal values of the F *A* tensor, see text). [b] The optimized geometry and the all electron ae^F and ae^G basis sets for fluorine and the all-electron ae^B basis set for titanium were used throughout (see Table 2 for a description).

presented. The two sets of experimental isotropic values for carbon and hydrogen correspond to direct experimental results from ref 24 and to the hypothetical nonvibrating planar molecule, cf. refs 15 and 18, respectively. As we can see, the vibrational corrections have been estimated to be quite significant, about 25.2−28.0 MHz, for carbon, while for hydrogen the vibrational effects are not as significant (about 5 MHz). As far as the calculated hydrogen isotropic term is concerned, the LSD calculation (as used for Table 8) appears to be a bit low −53.9 MHz), as mentioned earlier. The BP, PW91, and PW86 functionals give corrections in the right direction, with the BP value of −67.0 MHz coming quite close to the "experimental" value for the static molecule, −70 MHz. This tendency of underestimation by LSD is much stronger even for ^{13}C, the GGA functionals all correcting quite nicely.

Turning next to the anisotropic *A* tensors, we note that the differences between the various density functionals are not significant at both H and C. On C, the *zz* and the (equal by symmetry) in-plane components are overestimated by some 25−30%. Given the significant reduction (40%) of the isotropic hfsc of C by correcting the experimental number for vibrational effects, it is obvious that vibrational averaging may cover much of the difference and will have to be taken into account for a definitive assessment.

For the anisotropic *A* tensor on H, the GGA functionals also hardly change the LSD result. The comments in the previous section therefore hold for the GGA results for the anisotropic *A* tensor as well. In summary, the agreement with experiment is good for the isotropic hfs constants, in particular for the BP functional, and is satisfactory, given the lack of vibrational corrections, for the anisotropic *A* tensors. From preliminary investigations on analogous organic radicals, it appears that this conclusion is general; the anisotropic hf structures are, in general, much less dependent on the choice of functional and appear to be overestimated in the static structures, the isotropic couplings are well reproduced only by including nonlocal corrections, while no clear preference for one of the GGA's for the description of the isotropic hf couplings could be established.

We turn next to an investigation of the effect of the nonlocal corrections on the TiF_3 radical, which are reported in Table 10. The optimized geometry and two different and extensive basis sets (ae^F and ae^G) were used for the fluorine atoms, and only the most extensive basis set was used for titanium (see Table 2 for a description). The Ti isotropic hfs constant is rather insensitive to the density functional used. It is rather high compared to the experimental value, as observed before.[1] We have verified that averaging over the bending (umbrella) vibration, which is very soft, would lower this value. Since slight lengthening of the Ti−F bond also lowers the Ti isotropic hfsc considerably (to −164.1 MHz upon lengthening by 0.10 Å), both the umbrella motion and anharmonicity in the symmetric stretch vibration (r_0 will be larger than r_e) will make corrections in the right direction. The calculated static Ti isotropic hfsc is therefore considered quite satisfactory. (NB Table 6 in ref 1 shows the lowering of the $A_{contact}$ upon Ti−F bond lengthening,

but the values refer to a frozen core calculation and are therefore ca. 60 MHz too high).

The fluorine isotropic hf couplings vary only slightly with the density functional that is used, and they are always very small in magnitude. In view of the somewhat better results of the gradient corrected functionals so far, one might prefer the GGA values in the best basis, i.e., very small positive value of 5−10 MHz. These values of A_{iso} are in very nice agreement with the isotropic *A* value of 8 MHz which is obtained from experiment if we use for the experimental principal *A* values the signs that come out of the calculation, i.e., a different sign for the *zz* component than for the in-plane components. However, when adding the isotropic part to the principal values of the traceless *A* tensor for the PW91 and PW86 functionals, the agreement with experiment would deteriorate compared to the LSD value. For instance, the A_{zz} component would become smaller than the experimentally well-established value of ca. 45 MHz. We conclude that the LSD and, among the gradient corrected functionals, BP give good agreement with experiment. In view of the fact that the *A* tensor is small anyway, which is well reproduced by all of the functionals, one also may conclude that agreement with experiment is satisfactory for all of the functionals. The DFT calculations do reproduce the experimental fact of only slight delocalization of the unpaired spin to the F ligands, with a very good order of magnitude estimate of the resulting small *A* tensor.

4. Discussion and Conclusions

In the Kohn−Sham formulation of density functional theory, one is basically working in terms of a molecular orbital model. It is possible to understand how the effects of electron correlation are incorporated in this model. For instance, the effect of electron correlation is to reduce the conditional probability of finding a second electron in the neighborhood of a given one (creation of the Coulomb hole surrounding an electron). The Fock operator contains, in an orbital-dependent form, the potential due to the Fermi hole but it lacks the Coulomb hole potential. In contrast, the Kohn−Sham potential incorporates, in addition to the potential due to the averaged Fermi hole, the potential of the Coulomb hole.[46] This makes it understandable how an orbital model still incorporates correlation effects on an observable property such as the electronic density. The implication is that the interpretation of various effects will be couched in orbital terms in a KS calculation, even if they would traditionally be considered as correlation effects for not being present in the Hartree−Fock treatment.

In the present paper we are dealing with spin densities, which will be interpeted in terms of spin polarization effects on the orbitals in the KS calculation. We may contrast the KS picture for the generation of finite spin density at the H nucleus of the D_{3h} π radical CH_3 with the traditional VB picture. Consider an isolated CH_3 fragment radical with one electron occupying the $2p_z$ carbon orbital perpendicular to the plane of the three trigonal bonds. There are two VB configurations for the description of the C−H σ bond, which would be equally important in the absence of the unpaired electron in $2p_z$: (a) a spin α electron in the carbon σ hybrid orbital and a spin β electron in the hydrogen 1s orbital; (b) vice versa. The presence of the $2p_z$ electron, however, makes the two configurations no longer equally probable. Because of the favorable exchange interaction between the π electron and the carbon σ electron, when the spins are parallel (both α), configuration (a) is slightly preferred. This configuration has a β electron in H 1s; for this reason, the spin density at the proton is negative, as is the hyperfine coupling constant.

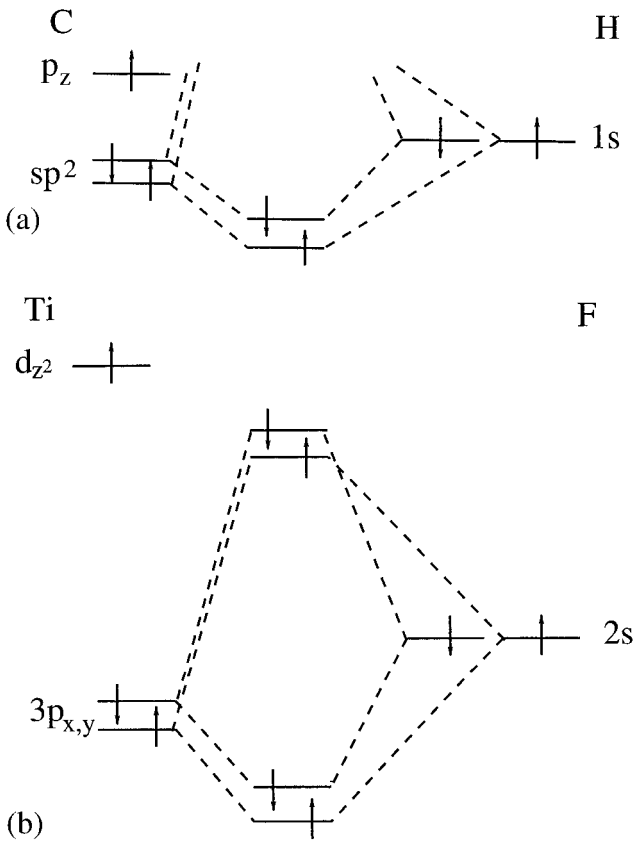

Figure 3. Orbital interaction diagram for CH_3 and TiF_3.

We shift now to an MO interaction picture, as illustrated in Figure 3. The 1s hydrogen orbitals interacting with the carbon sp^2 hybrid orbitals are shown. The α spin electron in the carbon p_z orbital implies that there is a higher α spin density at carbon, which means that the exchange operator (roughly proportional to $-[\rho^{\alpha}]^{1/3}$) creates a stabilizing field for the α occupied sp^2 orbital. When the hydrogen 1s spin orbitals mix with the carbon sp^2 spin orbitals, the stabilization of the $sp^2\alpha$ spin orbital relative to the $sp^2\beta$ spin orbital will lead to more sp^2 character in the α-spin bond orbital and relatively more hydrogen 1s character in the β-spin bond orbital. This is the spin polarization mechanism for creating an excess β spin density at the H nucleus in the prototype π radical CH_3. We have seen above that with the present GGA functionals the spin polarization is described fairly accurately in CH_3.

A similar simple MO picture can be applied to the description of the spin polarization in the TiF_3 molecule. The orbital interactions are displayed in Table 4, where we show the one-electron eigenfunctions and eigenvalues for the unrestricted calculation performed on TiF_3, using the basis set DZ (1s frozen) described in Table 2. Table 7 collects the individual contributions of the various orbitals with fluorine s components to the Fermi contact term $A_{contact}$ of the ^{19}F hyperfine tensor of TiF_3. The fluorine 2s orbital interacts only weakly with other orbitals, the energetic distance to all other orbitals being fairly large. In Table 4 we easily recognize the block of predominantly F 2s orbitals ((96%) at ∼−29 eV. The most important interaction is with the Ti $3p_{x,y}$ orbitals ($3e_1'$ at ∼−40 eV). This interaction is depicted in Figure 3. In this case, the exchange interaction with the unpaired α-spin electron which occupies the $3d_{z^2}$ orbital stabilizes the α-occupied $3p_{x,y}$ orbitals. As a consequence, the interaction with the fluorine 2s orbital is such that the α-spin "bonding" orbital $3e_1'\uparrow$ has a somewhat smaller admixture of F 2s than the β-spin bonding orbital $3e_1'\downarrow$. This leads, in agreement

with Table 7, to the largest negative contribution to the spin density at the F nucleus from the nominally Ti 3p orbital. TiF_3 however differs from the CH_3 case in that now also the antibonding combinations $4e_1'$, which are mostly F 2s, are occupied. In those orbitals the relative magnitude of the contributions of the F 2s in the spin-up and spin-down orbitals will be reversed compared to those in the bonding orbitals; therefore, the spin polarization effect of the "bonding" $3e_1'$ is partially annihilated by the opposite polarization of the "antibonding" $4e_1'$ orbitals. (The interactions are very weak, as is evident from the very slight mixings in Table 4, so "bonding" and "antibonding" denote the sign of the interactions, in-phase or out-of-phase, rather than genuine bonding or antibonding energetic effects). There is also slight mixing between the F 2p set of orbitals, at about -10 to -12 eV, and the F 2s at ca. -29 eV. With exactly the same mechanism as described above this leads to analogous negative/positive polarizations in the $5a_1'$/$6a_1'$ pair. The $4e_1'$/$5e_1'$ pair should also show such negative/positive polarization effects, but the negative effect is not visible in the $4e_1'$, it only diminishes the positive polarization this orbital has due to the aforementioned mixing with Ti $3p_{x,y}$. This completes the enumeration of all of the important contributions to the F 2s spin polarization. It is obvious now that the A_{contact} from the unpaired spin orbital $7a_1'$ ($+24.6$ in restricted case, $+20.1$ MHz in the unresticted case) has hardly any relation to the actual hyperfine splitting constant, which is dominated by spin polarization effects. The calculations with the F 1s unfrozen, also shown in Table 7, demonstrate the importance of the spin polarization of the 1s shell and have been commented upon above.

The spin polarization effects of the F 2s, being related to the interaction of the F 2s with metal orbitals and with F 2p combinations of the right symmetry depend on system-dependent details such as the type of metal and the geometry of the coordination (for instance overlap of F 2s with neighboring F 2p) and cannot be generalized in rules such as the McConnell relation between H hfsc and spin density on the neighboring C atom in aromatic radicals. In the aromatic radicals the relation between a H atom and the neighboring C atom in the aromatic ring *is* very much the same in different systems.

Summarizing, we come to the following conclusions.

(a) The DFT calculations lead to fairly accurate spin densities, both at the nucleus as evidenced by the isotropic *A* values (arising to first order from the Fermi contact interaction) and with regard to the Y_{2m}/r_N^3 moments with respect to nucleus *N* (the first-order contribution from the dipolar interaction). Differences between the local-density approximation (LSD) and the GGA's are not very striking, but if they exist, such as for the A_{iso} of ^{13}C in CH_3, the GGA's usually perform better, though not consistently so (cf. the too small A_{zz}^{F} for PW86). The best functional for the investigated systems seems to be BP. The level of agreement is such that vibrational averaging effects need to be taken into account in order to make a further assessment of the accuracy of the DFT calculations. The tendency of the DFT approach, noted earlier,[20,21] to overestimate the covalency and therefore to give errors in the electronic spin density distribution, has not been confirmed for the TiF_3 system. It may have arisen, as suggested by the authors, from limitations in the basis sets or to the frozen core approximation.[20]

(b) The spin polarization effects that give rise to both the isotropic *a* value and the anisotropic *A* tensor are of rather intricate nature. Furthermore, two-center contributions are quite important. For the anisotropic *A* tensor, various effects, polarization of all occupied 2p orbitals ($2p_\sigma$, $2p_\pi^{ip}$, $2p_\pi^{\perp}$), two-center contribution from the unpaired spin density on Ti contribute significantly. For the isotropic *a* value we have noted that even polarization of the lowest occupied shell (F 1s) is very important. An all-electron treatment (no frozen cores allowed) is necessary. Basis set requirements are rather stringent. The implication is that the measured values for both *a* and the full *A* tensor do not give very direct information on the electronic structure. They would be difficult to interpret without electronic structure calculations.

(c) Although ESR data yield in principle detailed information concerning the electronic structure, both the present paper and the previous one[1] demonstrate the usefulness, if not necessity, of the combination of experimental and theoretical treatment for a full interpretation of the message conveyed by the measured data. In the TiF_3 case, the calculations suggest opposite signs of the F *A* tensor principal values in the *z* and *x,y* directions, respectively. Since equal signs had been assumed originally,[2] the experimental isotropic *A* value has been revised accordingly.

(d) In view of their efficiency and the demonstrated accuracy, the DFT-GGA calculations hold great promise for the elucidation of ESR data of complex systems such as metallic centers in systems of biological interest. The recent DFT implementation of van Lenthe et al.[48] of the calculation of hyperfine splitting constants with relativistic effects taken into account within the zero-order regular approximation for relativistic effects[49] enables heavy elements to be treated as well, although further development will be required to treat relativistic effects (notably spin−orbit coupling) and spin-polarization effects simultaneously.

Acknowledgment. We are grateful to the European Science foundation for a visitors grant to P.B. under the REHE program.

References and Notes

(1) Belanzoni, P.; Baerends, E. J.; van Asselt, S.; Langewen, P. B. *J. Phys. Chem.* **1995**, *99*, 13094.
(2) DeVore, T. C.; Weltner, W., Jr. *J. Am. Chem. Soc.* **1977**, *99*, 4700.
(3) Balagopalakrishna, C.; Kimbtough, J. T.; Westmoreland, T. D. *Inorg. Chem.* **1996**, *35*, 7758.
(4) Mabbs, F. E.; Collison, D. *Electron Paramagnetic Resonance of d Transition Metal Compounds*; Elsevier: Amsterdam, 1992.
(5) Eriksson, L. A.; Malkina, O. L.; Malkin, V. G.; Salahub, D. R. *J. Chem. Phys.* **1994**, *100*, 5066.
(6) Kong, J.; Eriksson, L. A.; Boyd, R. J. *Chem. Phys. Lett.* **1994**, *217*, 24.
(7) Eriksson, L. A.; Malkina, O. L.; Malkin, V. G.; Salahub, D. R. *Int. J. Quantum Chem.* **1994**, *52*, 879.
(8) Barone, V.; Adamo, C.; Russo, N. *Int. J. Quantum Chem.* **1994**, *52*, 963.
(9) Ishii, N.; Shimizu, T. *Chem. Phys. Lett.* **1994**, *225*, 462.
(10) Malkin, V. G.; Malkina, O. L.; Eriksson, L. A.; Salahub, D. R. In *Theoretical and Computational Chemistry*; Politzer, P., Seminario, J. M., Eds.; Elsevier: Amsterdam, The Netherlands, 1995; Vol. 1, to be published.
(11) Chipamn, D. M. *J. Chem. Phys.* **1983**, *78*, 3112.
(12) Feller, D.; Davidson, E. R. *J. Chem. Phys.* **1984**, *80*, 1006.
(13) Carmichael, I. *Chem. Phys.* **1987**, *116*, 351.
(14) Chipman, D. M.; Carmichael, I.; Feller, D. *J. Phys. Chem.* **1991**, *95*, 4702.
(15) Barone, V.; Grand, A.; Michino, C.; Subra, R. *J. Chem. Phys.* **1993**, *99*, 6787.
(16) Perera, S. A.; Salemi, L. M.; Bartlett, R. *J. Chem. Phys.* **1997**, *106*, 4061.
(17) Nakatsuji, H.; Ehara, M.; Momose, T. *J. Chem. Phys.* **1994**, *100*, 5821.
(18) Chipman, D. M. In *Quantum Mechanical Electronic Structure Calculations*; Langhoff, S. R., Eds.; Kluwer: Netherlands, 1995; pp 109−138.
(19) Feller, D.; Davidson, E. R. In *Molecular spectroscopy, Electronic Structure and Intermolecular Interactions*; Maksic, Z. B., Ed.; Springer: Berlin, 1991; Vol. 3.
(20) Swann, J.; Westmoreland, T. D. *Inorg. Chem.* **1997**, *36*, 5348.
(21) Penfield, K. W.; Gewirth, A. A.; Solomon, E. I. *J. Am. Chem. Soc.* **1985**, *107*, 4519.

(22) Geurts, P. J. M.; Bouten, P. C. P.; van der Avoird, A. *J. Chem. Phys.* **1980**, *73*, 1306.
(23) Aarnts, M.; Wilms, M.; Peelen, K.; Fraanje, J.; Goubitz, K.; Hartl, F.; Stufkens, D. J.; Baerends, E. J.; Vleck, A., Jr. *Inorg. Chem.* **1996**, *35*, 5468.
(24) Fessenden, R. W. *J. Chem. Phys.* **1967**, *71*, 74.
(25) Baerends, E. J.; Ellis, D. E.; Ros, P. *Chem. Phys.* **1973**, *2*, 42.
(26) Baerends, E. J.; Ros, P. *Int. J. Quantum Chem.* **1978**, *S12*, 169.
(27) Baerends, E. J.; Ros, P. *Chem. Phys.* **1973**, *2*, 51.
(28) Keijzers, C. P. Ph.D. Thesis, Nijmegen, 1974.
(29) van Asselt, S. Master's Thesis, Vrije Universiteit, Amsterdam, 1984.
(30) Langewen, P. B. Master's Thesis, Vrije Universiteit, Amsterdam, 1985 (in Dutch).
(31) Snijders, J. G.; Vernooijs, P.; Baerends, E. J. *Atom Data Nucl. Data Tables* **1982**, *26*, 483.
(32) Vosko, S. H.; Wilk, L.; Nusair, M. J. *Can. J. Phys.* **1980**, *58*, 1200.
(33) Becke, A. D. *Phys. Rev.* **1988**, *A38*, 3098.
(34) Perdew, J. P. *Phys. Rev.* **1986**, *B33*, 8822.
(35) Perdew, J. P. *Phys. Rev.* **1986**, *B34*, 7046.
(36) Perdew, J. P.; Wang, Y. *Phys. Rev.* **1992**, *B45*, 13244. Perdew, J. P. In *Electronic Structures of Solids*; Zieschle, P., Eschrig, H., Eds.; Adademie: Berlin, 1991. Perdew, J. P.; Chevary, J. A.; Vosko, S. H.; Jackson, K. A.; Pederson, M. R.; Singh, D. J.; Fiolhais, C. *Phys. Rev.* **1992**, *B46*, 6671.
(37) Perdew, J. P.; Wang, Y. *Phys. Rev.* **1986**, *B33*, 8800.
(38) Versluis, L.; Ziegler, T. *J. Chem. Phys.* **1988**, *88*, 322.
(39) Pryce, M. H. L. *Proc. Phys. Soc. A* **1950**, *63*, 25.
(40) Herman, F.; Skilman, F. *Atomic Structure Calculations*; Prentice-Hall, Inc.: New York, 1963.
(41) Gribnau, M. Unpublished.
(42) Carrington, A.; McLachlan, A. D. *Introduction to Magnetic Resonance*; Harper Int. Ed.: New York, 1969.
(43) *Handbook of Chemistry and Physics*, 58th ed.; CRC Press: Boca Raton; p B270−B354.
(44) Case, D. A.; Karplus, M. *J. Am. Chem. Soc.* **1997**, *99*, 6182.
(45) Weber, J.; Goursot, A.; Pénigault, E.; Ammeter, J. H.; Bachmann, J. *J. Am. Chem. Soc.* **1982**, *104*, 1491.
(46) Baerends, E. J.; Gritsenko, O. *J. Phys. Chem. A* **1997**, *101*, 5383.
(47) Weltner, W., Jr. *Magnetic Atoms and Molecules*; Dover Publications, Inc.: Mineola, NY, 1983 and references therein.
(48) van Lenthe, E.; van der Avoird, A.; Wormer, P. E. S. *J. Chem. Phys.* **1998**, *108*, 4783.
(49) van Lenthe, E.; Baerends, E. J.; Snijders, J. G. *J. Chem. Phys.* **1993**, *99*, 4597.